



University of HUDDERSFIELD

University of Huddersfield Repository

Gong, Cencen, Iwnicki, Simon and Bezin, Yann

The interaction between railway vehicle dynamics and track lateral alignment

Original Citation

Gong, Cencen, Iwnicki, Simon and Bezin, Yann (2015) The interaction between railway vehicle dynamics and track lateral alignment. Proceedings of the Institution of Mechanical Engineers, Part F: Journal of Rail and Rapid Transit. ISSN 0954-4097 (In Press)

This version is available at <http://eprints.hud.ac.uk/23224/>

The University Repository is a digital collection of the research output of the University, available on Open Access. Copyright and Moral Rights for the items on this site are retained by the individual author and/or other copyright owners. Users may access full items free of charge; copies of full text items generally can be reproduced, displayed or performed and given to third parties in any format or medium for personal research or study, educational or not-for-profit purposes without prior permission or charge, provided:

- The authors, title and full bibliographic details is credited in any copy;
- A hyperlink and/or URL is included for the original metadata page; and
- The content is not changed in any way.

For more information, including our policy and submission procedure, please contact the Repository Team at: E.mailbox@hud.ac.uk.

<http://eprints.hud.ac.uk/>

THE INTERACTION BETWEEN RAILWAY VEHICLE DYNAMICS AND TRACK LATERAL ALIGNMENT

Cencen Gong, Simon Iwnicki and Yann Bezin
 Institute of Railway Research, University of Huddersfield
 Queensgate, Huddersfield, Yorkshire, United Kingdom, HD1 3DH
 E-mail address: u1273131@hud.ac.uk

Abstract

Track geometry deteriorates with traffic and needs to be regularly restored by tamping or other methods. As the deterioration is mainly in the vertical direction this aspect has been more widely studied and models developed but track lateral deterioration is not as well understood. This research aims to develop a method for analysing and predicting lateral deterioration of railway track caused by traffic, and to investigate the influences of different railway vehicles, running speeds, traffic mix and wheel-rail contact conditions.

1 VEHICLE-TRACK LATERAL MODEL

Track condition has a significant influence on the behaviour of the railway system in terms of ride safety, maintenance and passenger comfort. However, in practice it is physically impossible to eliminate track irregularity. It is therefore very important to understand the mechanism of the track deterioration to be able to predict development of track irregularities for reducing the life-cycle cost of the railway system and designing new track structures [1]. The deterioration of track alignment is usually measured by railway infrastructure managers using a Track Recording Coach (TRC). Various track vertical settlement models have been developed in order to predict the rate of change of vertical track level in many countries [2]. However, the mechanisms involved and the triggering limits in terms of lateral vehicle-track interaction dynamics are not very well understood. The limit of track lateral resistance still used by most railway organisations today was defined by Prud'homme [3] in 1967. The vehicle-track lateral dynamic interaction model in this work is established as the overall model scheme shown in Figure 1-1. The vehicle-track lateral interaction can be effectively modelled based on two main parts, which are the vehicle-track interaction model and the track lateral deterioration model. The vehicle-track interaction model is an existing Multi-body System (MBS) model, in this case the VAMPIRE simulation tool. The outputs forces from the Vampire simulation are then used as the inputs to a Finite Element (FE) track model.

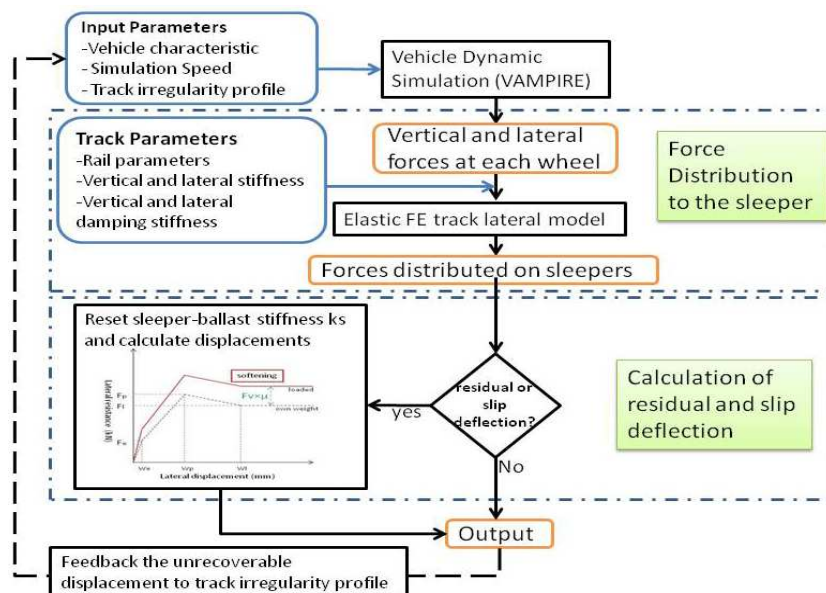


Figure 1-1 Vehicle-track lateral deterioration model scheme

The VAMPIRE simulations use input data selected to match conditions observed on selected track sections as shown in Table 1-1. Outputs are the resolved vertical and lateral forces at each wheel of the vehicle onto the rails.

Table 1-1 Simulation inputs and outputs

Track irregularity data	Measured track data
Vehicles	Veh.1 – Class 390; Veh.2 – Class 221; Veh.3 – MarkIII Veh.4 – FEAB, FSAO, FTAI, KFAF laden; Veh.5 – FEAB, FSAO, FTAI, KFAF tare; Veh.6 – IPAV laden; Veh.7 – IPAV tare
Calculation time step	0.001 s
Output time step	0.004s for passenger vehicles Veh.1 – Veh.3 0.005s for 4-axle freight vehicles Veh.4 – Veh.5 0.009s for 2-axle freight vehicles Veh.6 – Veh.7
Speed	100mph (44.70 m/s) for passenger vehicles 75mph (33.528m/s) for 4 axle freight vehicles 45mph(20.117m/s) for 2 axle freight vehicles
Coefficient of friction	0.4 for passenger vehicles, 0.3 for freight vehicles
Contact file	Uic60-20-worn_br-p8-worn for passenger vehicles Uic60-20-worn_br-p10 for 4-axle freight vehicles Uic60-20-worn_br-p5 for 2-axle freight vehicles
Creep law	Friction coefficient 0.3 Nonlinear creep law

The FE track lateral model shown in Figure 1-2 is built in MATLAB. It consists in 3-lateral/3-vertical degrees of freedom per sleeper element, including two extra nodes for the rail beam in between two sleepers which was determined to give sufficiently accurate peak displacement of the sleeper rigid body mass while maintaining reasonable calculation speed.

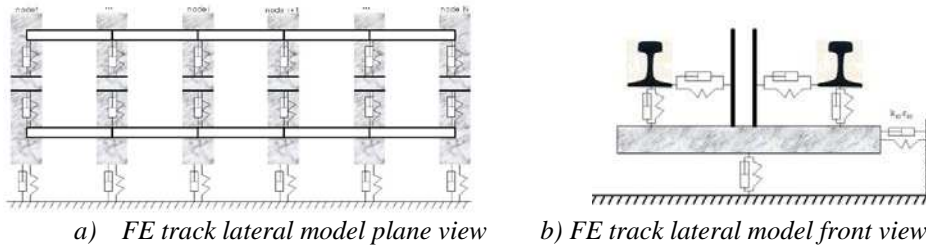


Figure 1-2 FE track lateral model

The non-linear characteristic of the lateral resistance is shown in Figure 1-3 (a), which has been determined from experimental programs by BR Research [4], DB [5], and TU Delft [6]. The simplified non-linear characteristic illustrated in Figure 1-3 (b) is employed in the actual track model in order to make the calculation process easier.

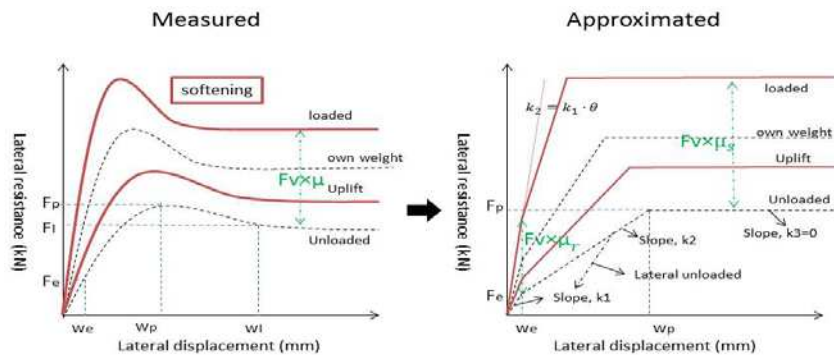


Figure 1-3 Track lateral resistance characteristic

F_e and w_e represent the elastic breaking force and displacement, and F_e varies with different distributed vertical loads. F_p and w_p are respectively the break-away resistance and displacement, which are the force and displacement required to overcome the static friction and initiate motion [7]. They can be seen as the starting point when the sleeper slides laterally on the ballast bed. θ is the residual deflection stiffness softening factor and 0.98 to 0.99 is found to be appropriate for consolidated track. F_v is the vertical distributed force from the rails to the sleeper. Even small forces can cause residual deflections therefore, it is not sensible to use the actual friction

coefficient between the sleeper and ballast in the residual deflection calculation. For example, the lateral forces are usually less than 5 kN on straight track, and using the actual friction coefficient which create the dynamic elastic breaking force of more than 20 kN will not help capture any small accumulated residual deflection after a number of passes. Therefore, a much smaller coefficient is defined and used in the model for residual deflection calculation. μ_r is the ‘friction coefficient’ between the sleeper and ballast layer for the residual deflection determination which is 3% of the actual sleeper-ballast friction coefficient μ_s . The parameters selected for the track model is shown in Table 1-2 selected from some track lateral test results [8] [9] [10] [11] [12].

Table 1-2 Track parameters

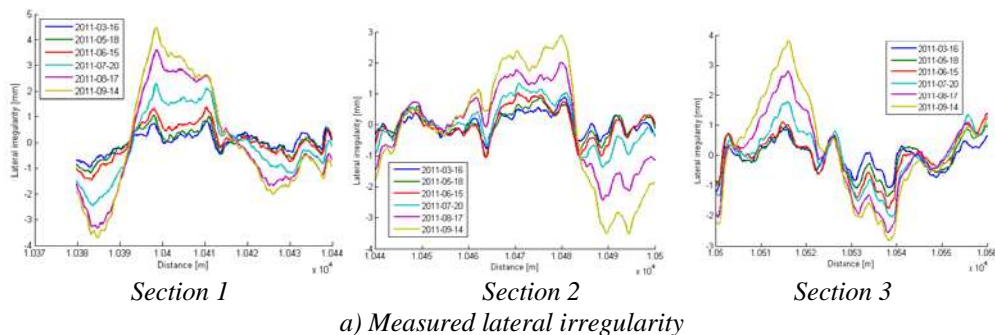
	Symbol	Units	Value
Young modulus	E	N/m ²	2.108×10^{11}
Section mass of UIC60 rail	m_r	kg	60
G44 concrete sleeper mass	m_s	kg	308
Sleeper spacing	s	m	0.6
Section moment of area about vertical axis	I_{zz}	m ⁴	5.123×10^{-6}
Section moment of area about horizontal axis	I_{yy}	m ⁴	3.038×10^{-5}
Rail pad lateral stiffness	k_{ry}	N/m	3.98×10^7
Rail pad lateral damping	c_{ry}	N · s/m	3×10^4
Rail pad vertical stiffness	k_{rz}	N/m	6.3×10^7
Rail pad vertical damping	c_{rz}	N · s/m	4×10^4
Sleeper-ballast lateral damping	c_{sy}	N · s/m	2.5×10^4
Sleeper-ballast vertical stiffness	k_{sz}	N/m	9×10^7
Sleeper-ballast vertical damping	c_{sz}	N · s/m	8×10^4
Elastic breaking displacement for weak track	w_e	m	0.01×10^{-3}
Elastic breaking force for weak track	F_e	N	40
Peak resistance displacement for weak track	w_p	m	3×10^{-3}
Peak resistance force for weak track	F_p	N	8×10^3
Residual deflection coefficient	μ_r	-	0.01
Friction coefficient	μ_s	-	0.3
Softening factor	θ	-	0.9985

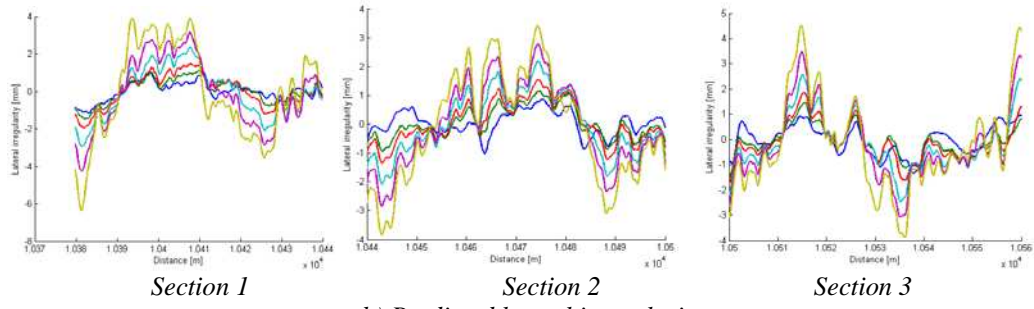
Table 1-3 is the traffic mix on the section of track used in the validation process and the traffic is considered evenly distributed within each time period.

Table 1-3 Traffic scenario for later simulation [13]

	Datasets	Veh.1	Veh.2	Veh.3	Veh.4	Veh.5	Veh.6	Veh.7
19/01/2011	D1	Wheelsets passages between two measured data sets						
16/03/2011	D2	16909	1258	308	946	657	46	32
18/05/2011	D3	19023	1416	346	1064	739	52	36
15/06/2011	D4	8454	629	154	473	329	23	16
20/07/2011	D5	10568	787	192	591	411	29	20
17/08/2011	D6	8454	629	154	473	329	23	16
14/09/2011	D7	8454	629	154	473	329	23	16

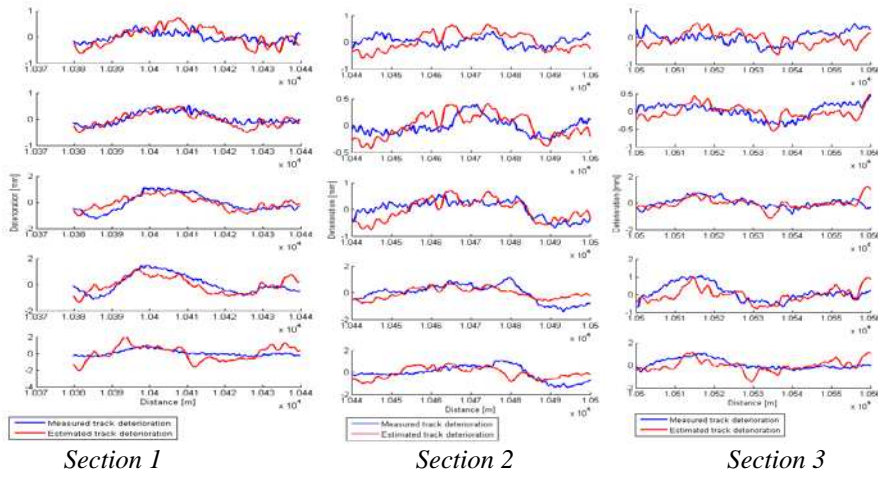
Figure 1-4 a) and b) are respectively the measured and predicted track lateral irregularity over three 60m track sections. The peak lateral deterioration and increase from one period to the other are well predicted.



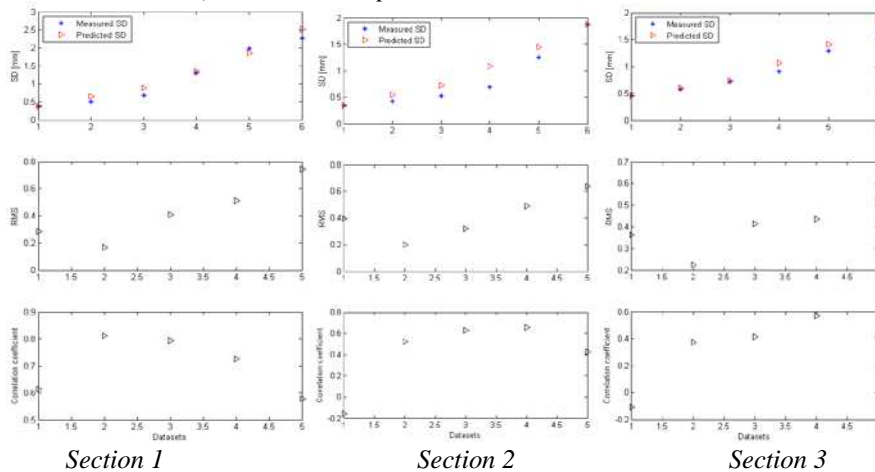


b) Predicted lateral irregularity
 Figure 1-4 Measured and predicted track irregularity comparison

Figure 1-5 a) shows the comparison between measured and predicted lateral deterioration change for three track sections, which is the difference between two consecutive time periods. Figure 1-5 b) illustrates the SD value of this section of track, as well as the RMS and correlation coefficient values of the measured and predicted lateral deterioration. The correlation coefficients for the first predictions are very low, because the long wavelength irregularity magnitudes are low and the short wavelength irregularities do not have a strong correlation. The RMS value indicates the magnitude of the difference between measured and predicted lateral deterioration, therefore, the bigger RMS value is the less accurate the prediction is. Correlation coefficient measures the linear correlation between the measured and predicted deterioration.



a) Measured and predicted lateral deterioration



b) Precision measures

Figure 1-5 Deterioration comparison and precision measurement

It can be found from RMS and correlation values for these three sets of results that the prediction is reasonably accurate for first 4 to 5 datasets, and become less accurate with increasing time since the RMS grows and correlation coefficient starts to drop. From the comparison of actual measured and predicted track lateral irregularities it can be found that there is an additional small wavelength irregularity of the predictions that does

not appear in the measured data. The PSD of the both measured and predicted lateral deterioration is calculated for these three sections of track. Aside of a good match for all low frequencies, the predicted deterioration includes a higher frequency component that does not exist in the real deterioration. This high frequency corresponds to a wavelength between 0.09259 to 0.1389cycle/m (6.17 to 10.8m) as shown in Figure 1-6. As the vehicle dynamic forces are the only input to the track model, this is surely caused by a vehicle dynamic mode that can be excited by different factors (e.g. the wheel-rail kinematic modes).

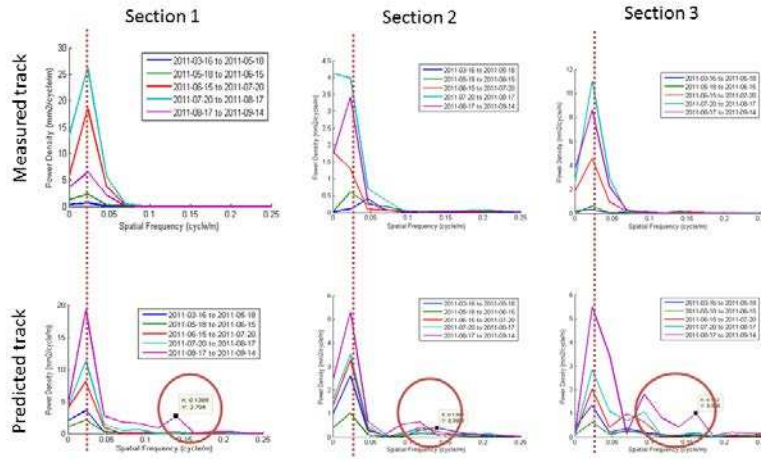


Figure 1-6 PSD results of measured and predicted lateral deterioration

If the 3 to 10.8 m wavelengths are filtered out from the results, the SD values are much better matched, meanwhile, the RMS and correlation coefficient values indicate a much more accurate prediction results with the filtered data shown in Figure 1-7. Therefore, it is important to understand why this short wavelength deterioration does not exist in the actual track lateral deterioration, despite the fact that the vehicle dynamic forces are predicted in this short wavelength range.

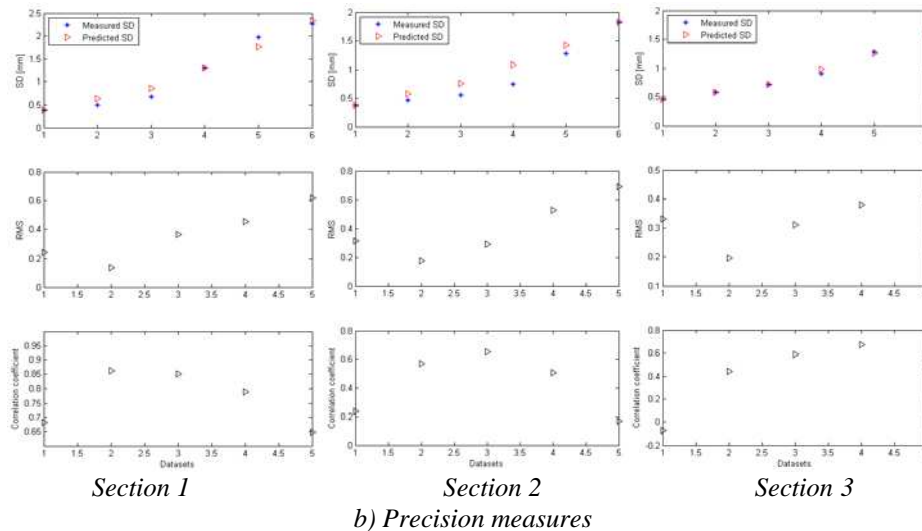
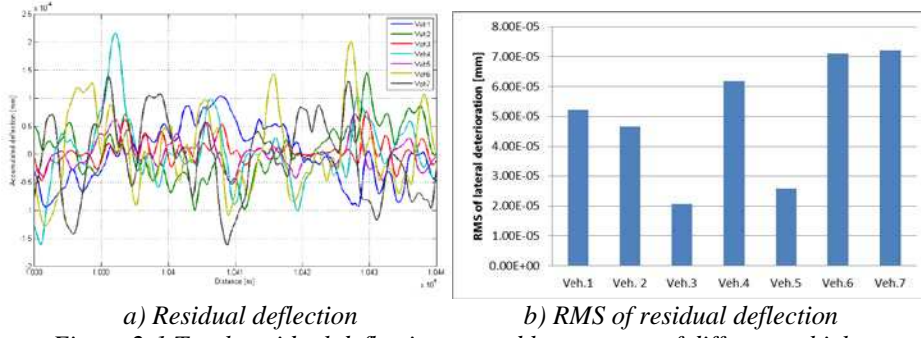


Figure 1-7 Deterioration comparison and precision measurement

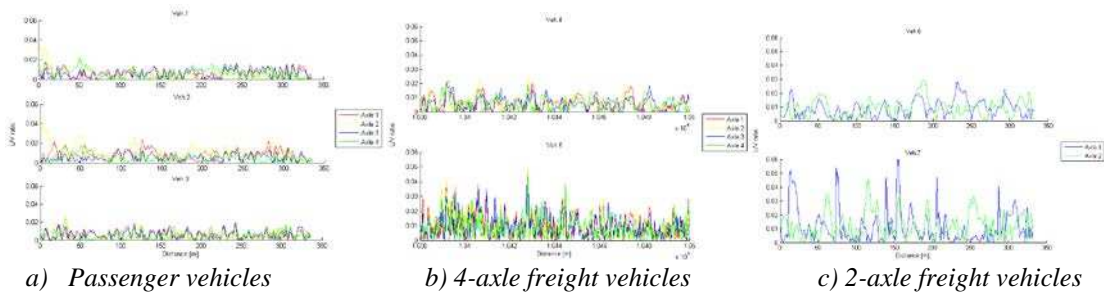
2 EFFECT OF DIFFERENT VEHICLES

The effect of different vehicles running on one section of measured track and the influence of the running speed of the most common vehicle (Class390) on the track lateral deterioration are discussed. The simulation results for the track deterioration caused by different vehicles for one vehicle pass on the tangent line is shown in Figure 2-1. For quantities varying both positively and negatively like track deterioration, RMS value is a good measure of the amplitude.



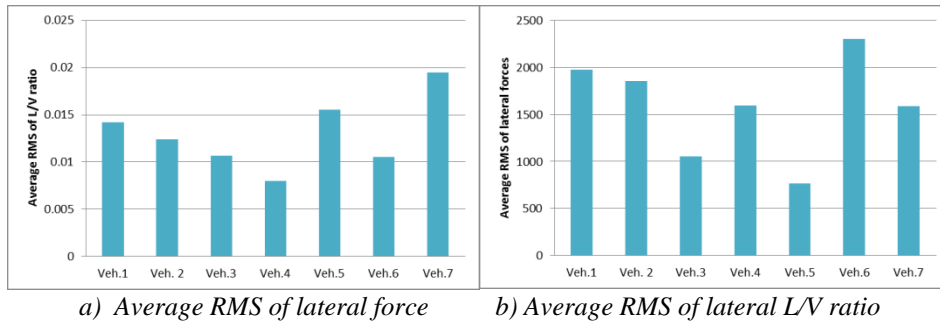
a) Residual deflection
b) RMS of residual deflection
Figure 2-1 Track residual deflection caused by one pass of different vehicles

It can be found that generally the freight vehicles Veh.6 and Veh.7 have the biggest impact. Since the L/V ratio is considered the biggest impact factor of the residual deflection, the dynamic L/V loading ratio from all vehicles are calculated and shown in Figure 2-2.



a) Passenger vehicles
b) 4-axle freight vehicles
c) 2-axle freight vehicles
Figure 2-2 Lateral to vertical loading ratio delivered from vehicles to rail

Figure 2-3 is the summary of the mean L/V ratio from different vehicles. For the passenger vehicles Veh.1 to Veh.3 with similar static loads, Veh.1 has the biggest L/V ratio while Veh.3 has the smallest. Therefore, the resulted residual deflection by Veh.1 is the biggest as in Figure 2-1 b). On the other hand, the laden freight vehicles have much smaller L/V ratio than the tare ones, yet create bigger residual deflections. The reason is that the laden vehicles have much bigger lateral forces. Therefore, it can be deduced that the residual deflection depends on both lateral forces and L/V loading ratios.



a) Average RMS of lateral force
b) Average RMS of lateral L/V ratio
Figure 2-3 Summary of average RMS of lateral forces and L/V ratio of different vehicles

Considering the dynamic forces experienced by each sleeper, the residual deflection under a certain lateral and vertical forces can be calculated as described in Figure 2-4. Therefore, the lateral residual deflection can be calculated by Equation 1.

$$w_r = w_{re} - w = \left(\frac{F_L - c_r \cdot w_{re}' - b}{k_2} \right) - \left(\frac{F_L - c_r \cdot w'}{k_1} \right) \quad \text{Equation 1}$$

Substitute the values in Figure 2-4 into Equation 1 and rearrange,

$$w_r = \frac{w_e}{\theta} \cdot \left(\frac{F_{Lstiff1} - \theta \cdot F_{Lstiff2}}{\mu_r \cdot [E_V] + F_e} - (1 - \theta) \right) \quad \text{Equation 2}$$

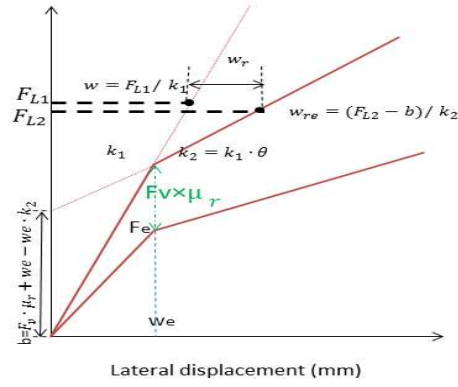


Figure 2-4 Residual deflection calculation

With the complicated vehicle-track dynamic interactions, it is very difficult to solve the equation and find out the force influence factor on the lateral residual deflection. If the damping is not considered, the only influence factors are the L/V loading ratio (F_L/F_V) and distributed lateral forces on the sleeper (F_L).

$$w_r = w_e \cdot \left(\frac{1}{\theta} - 1 \right) \left(\frac{1}{\frac{\mu_r}{\frac{F_{Lstiff}}{F_V}} + \frac{F_e}{F_{Lstiff}}} - 1 \right) \quad \text{Equation 3}$$

For vehicles with similar lateral forces, the vehicle with big L/V ratio creates more lateral deterioration. Meanwhile, with similar L/V ratio, vehicles with larger lateral forces leads to bigger lateral residual deflection. For vehicles with different L/V ratios and lateral forces, it is better to use the vehicle-track model to simulate the influences by the vehicles. For the track studied, the 2-axle vehicles lead to the biggest residual deflection for each vehicle pass, even though the speed limit for these vehicles is low.

3 EFFECT OF DIFFERENT RUNNING SPEED

The running speed of the vehicle has a very big influence on the vehicle-track dynamics, therefore, for different types of vehicles there are different speed limits. The most influential vehicle Veh.1 is selected to see how the running speed of the vehicle can influence the lateral residual deflection, and the speeds that will be discussed are shown in Table 3-1. All the results are captured under 1000 vehicle passes.

Table 3-1 Different vehicle running speed

	-20%	-15%	-10%	-5%	Original	+5%	+10%	+15%	+20%
mph	80	85	90	95	100	105	110	115	120
m/s	35.763	37.998	40.234	42.469	44.704	46.939	49.174	51.410	53.645

Figure 3-1 shows the resulted residual deflection under different speeds mentioned above. The thick lines indicate the lowest, original and highest speed respectively.

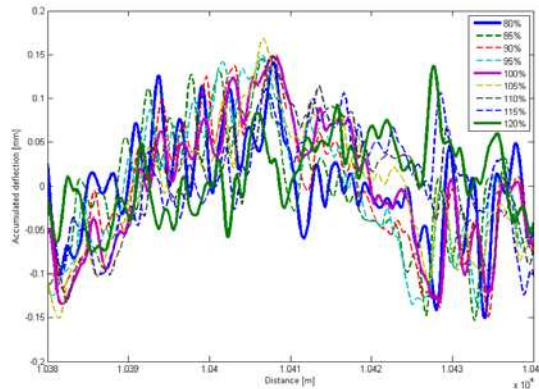
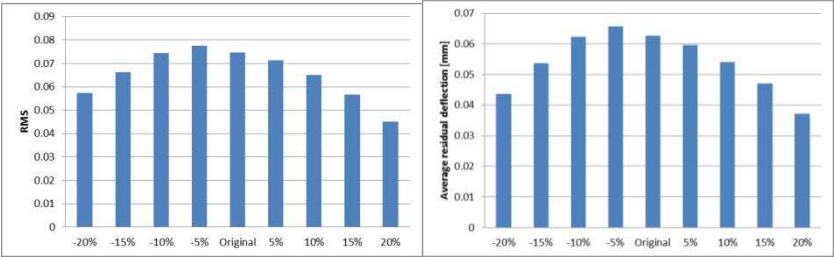


Figure 3-1 Residual deflection at different speed

Figure 3-2 illustrates the RMS of the residual deflections resulting from running the vehicle at different speeds. No clear trend can be found for the peak residual deflection, yet the average residual deflection is the biggest at 95 mph.



a) RMS of residual deflections b) Average residual deflections
 Figure 3-2 RMS and average residual deflection at different speed

It will be more interesting to look at the impact of the speed on the residual deflection in frequency domain. Figure 3-3 summarizes the lateral forces PSD peak changes in frequency domain.

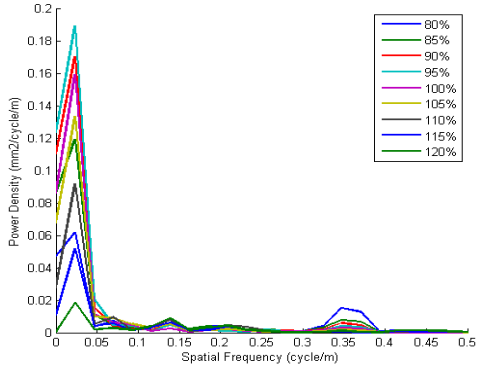
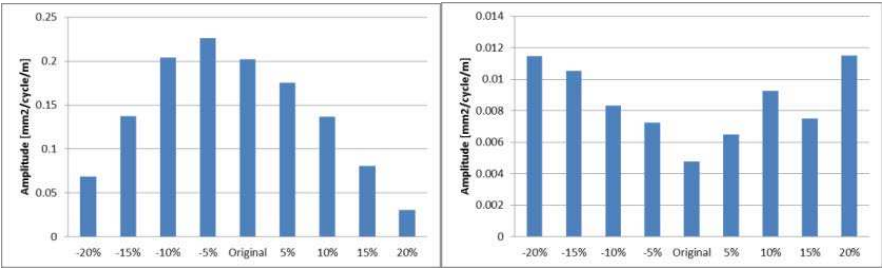


Figure 3-3 PSD of residual deflections resulted by different speeds

It can be found that the wavelengths of the first two peaks do not change significantly, while the power density of the residual deflection at these peaks does change. The change in the 1st peak of the PSD agrees with the result of average residual deflection change, while the 2nd PSD peak has the opposite trend. As the peak power density of the 1st peak has much bigger value than the 2nd one, there is more influence by the 1st peak on the lateral deflection.



a) Peak 1 b) Peak 2
 Figure 3-4 Two peak power densities change

The change of the vehicle speed does not necessarily bring a wavelength but an amplitude change to the residual deflection. There will be a critical speed that creates the peak residual deflection and reducing or increasing the vehicle speed (within permitted operational speed) can reduce the residual deflection at some point. For the Class390 vehicle this critical speed is around 95 mph (44.704 m/s).

4 EFFECT OF DIFFERENT TRAFFIC MIX

The effect of the different vehicles on the residual deflection taking into account the actual traffic mix by factoring the obtained residual deflection for one pass with the number of axle passes is shown in Figure 4-1. It shows that Veh.1 has the major influence on the lateral track irregularity growth compared to other vehicles.

This is due to the fact that this vehicle makes up more than 95% of the traffic on this section of the WCML, as shown in in Table 4-1.

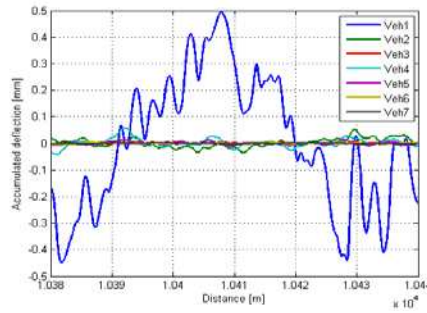


Figure 4-1 Residual deflection caused by different vehicles

Different vehicles have different dynamic behaviour thereby creating different lateral damage to the track. From the results shown in Figure 2-1 a), Veh.2 appears to create a lateral deterioration with a negative correlation to the deterioration created by Veh.1. Interestingly, a different traffic mix can help to reduce the lateral deterioration created by different vehicles. If the traffic pattern is altered between Veh.1 and Veh.2 the resulting changed D1 – D2 traffic is shown in the table below.

Table 4-1 Axle passages for each vehicle

	Veh.1	Veh.2	Veh.3	Veh.4	Veh.5	Veh.6	Veh.7
D1 – D2	19023	1416	346	1064	739	52	36
Changed D1 – D2	10219	10219	346	1064	739	52	36

Figure 4-2 shows the results of the track lateral deterioration under the actual and optimised traffic scenario. It can be seen that the lateral deterioration created by Veh.1 is almost opposite to the deterioration created by Veh.2, so more axle passages of Veh.2 can effectively reduce the deterioration created by Veh.1. The SD of the track section drops to 0.4283 from 0.5476 by changing the traffic mix.

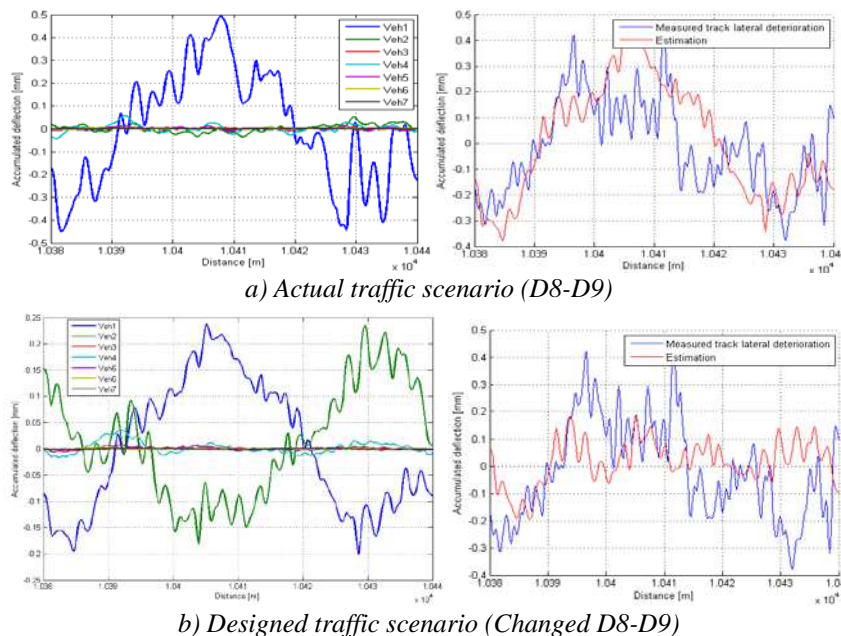


Figure 4-2 Track deterioration under actual traffic and designed traffic scenario

5 EFFECT OF DIFFERENT WHEEL-RAIL CONTACT

In reality there will be many different worn conditions of the rails and wheels. In order to see if the worn rail and wheel profiles makes a big difference to the vehicle-track dynamics, some comparison were made by running the vehicle-track lateral simulation with different combinations of wheel and rail profiles. The wheel-rail contact profiles discussed in this section are listed in Table 5-1. All worn rail profiles are in slightly worn condition for

wheel-rail contact set 1. The average worn wheel profiles of different vehicles running on ECML are obtained from the software VTISM [14] for wheel-rail contact set 2. The worn wheel profiles discussed in wheel-rail contact set 3 are different level of worn wheel profiles measured on one Class390 vehicle.

Table 5-1 Wheel-rail profile combination 1

	Num.	Rail profile	Wheel profile
Wheel-rail contact set 1	C1_1	New UIC60-20 rail	New br-p8 wheel
	C1_2	Measured worn UIC 60-20 rail 1	
	C1_3	Measured worn UIC 60-20 rail 2	
	C1_4	Measured worn UIC 60-20 rail 3	
Wheel-rail contact set 2	C2_1	New UIC60-20 rail	New br-p8 wheel
	C2_2		Class373 worn br-p8 wheel
	C2_3		Mark4 worn br-p8 wheel
	C2_4		Class 43 worn br-p8 wheel
Wheel-rail contact set 3	C3_1	Measured worn UIC 60-20 rail 1	Class390 worn br-p8 wheel 1
	C3_2		Class390 worn br-p8 wheel 2
	C3_3		Class390 worn br-p8 wheel 3
	C3_4		Class390 worn br-p8 wheel 4
	C3_5		Class390 worn br-p8 wheel 5

**the worn wheel from 1 to 5 indicates increasingly worn wheels*

The plots in Figure 5-1 are the resulting track lateral deterioration by using different wheel-rail contact sets listed in Table 5-1. Even if the wheels and rails are all the same original design profile with different worn condition, the dynamic influence this interface brings to the track lateral deterioration is crucial. The plots at the bottom in Figure 5-1 are the PSD plot of the track lateral deterioration with different wheel-rail contacts. It can be found that different worn wheel and rail profiles in all contact sets bring wavelength changes. In contact set 3, it can be found that the wheel wear leads to an obvious decrease of the long wavelength lateral deterioration. As a result, the low conicity created by the worn wheel profile brings smaller lateral forces to some extent. However, the life of railway wheels is usually limited by wear, and the wear between rail and wheel leads to problems in stability, life cycle cost and passenger comfort. This leads to the conflict between the best worn rail and wheel profile for track lateral deterioration and other aspects.

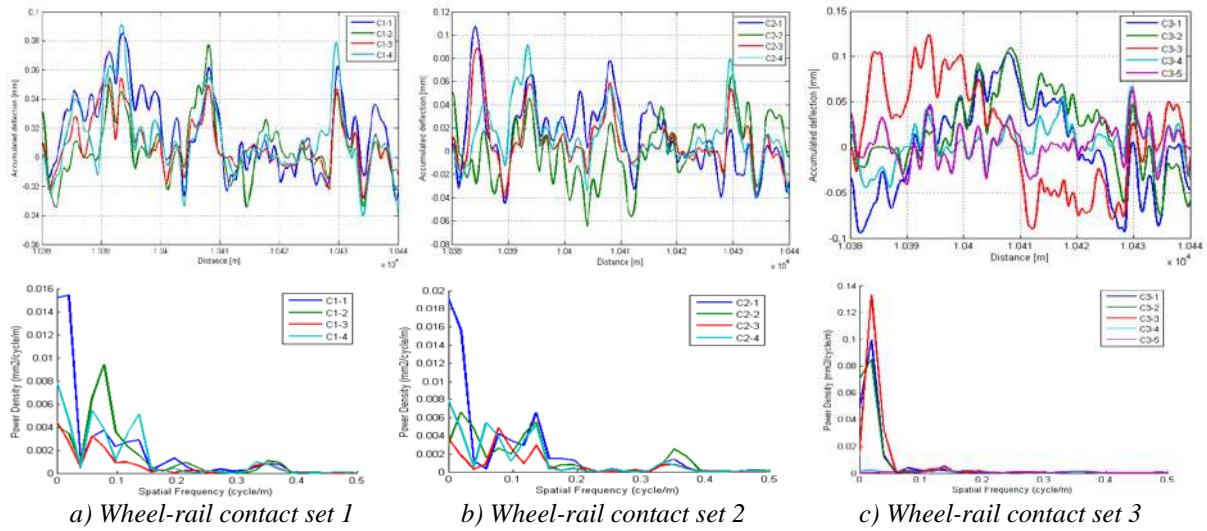


Figure 5-1 Track lateral deterioration with different wheel-rail contacts

6 CONCLUSIONS AND FUTURE WORK

Track lateral deterioration is a highly non-linear and complicated process which is not well understood. The level of lateral track irregularities is normally estimated by the Standard Deviation (SD) value which does not indicate specific peak deflections. A novel vehicle-track lateral dynamic interaction model has been established to simulate the link between dynamic behaviour of railway vehicles and track lateral alignment, and the model has been validated against recorded track data. It has been found that the model gives reasonably accurate prediction of the development of track irregularity, however it tends to additionally predict a short wavelength deterioration that is not seen in the actual track deterioration. The lateral damage caused by the vehicle to the track depends on

both L/V ratio and the lateral loads, yet it is a complicated dynamic process that cannot be easily expressed through a simple function. It is therefore more sensible to establish the damage from each vehicle to the track by carrying out a dynamic simulation. Two-axle freight vehicles are found to produce most lateral track damage due to their high axle load, simple suspension design and resulting dynamic behaviour. The change of the vehicle speed does not necessarily bring a wavelength change to the residual deflection but does create amplitude changes to the track deterioration. Within a certain speed range, there will be a critical speed that creates the peak residual deflection and reducing or increasing the vehicle speed can reduce the residual deflection at some point. The traffic mix can be optimised according to different vehicle dynamics in order to reduce the lateral deterioration. It can be found that the wheel and rail profiles play an extremely important role in the track lateral deterioration by influencing the vehicle-track lateral dynamics. Different rail and wheel worn profiles leads to totally different vehicle lateral dynamic forces. For a fixed worn rail and worn wheel on a particular type of vehicle, the increase of the wheel wear make the track lateral residual deflection smaller due to smaller conicity and lateral forces. Therefore, it is important to select the right measurement of the wheel and rail profiles, and find representative wheel-rail contact for the track section that need to be analysed, and better understanding of the rail-wheel wear can lead to a more accurate prediction result.

This model is proved to have an accurate prediction on the track lateral deterioration within roughly 8 months on a mainline railway with heavy traffic. The impact by different types of vehicles, vehicle running speeds and wheel rail contact conditions are discussed. For the further work, this model can be improved by taking into account additional factors such as the influence of longitudinal forces from the wheels to the rails, different weather and temperatures, subgrade and ground conditions, etc. The reason for the high frequency noise in the deterioration prediction is not understood yet and it should be discussed in terms of more accurate vehicle simulation results and more comprehensive rail and wheel worn profiles measured on the target track and vehicles. Furthermore, the sleeper-ballast lateral characteristics are not well understood and the references for them are quite limited. To improve on the present work it would be useful to carry out laboratory tests in order to capture more accurately track lateral stiffness and damping values as well as comprehensive non-linear characteristic of track lateral residual resistance behaviour.

7 REFERENCES

- [1] I. Makoto, "Track Technology Measurements of TRack Settlement and Its Prediction with Track Dynamic Model," *RTRI (Rail Technical Research Institute)*, vol. 16, pp. 41-46, 2002.
- [2] T. Dahlberg, "Some railroad settlement models—a critical review," *Proceedings of the Institution of Mechanical Engineers, Part F: Journal of Rail and Rapid Transit*, vol. 215, p. 289, 2001.
- [3] A. Prud'homme, "Resistance of The Track to Lateral Loads Exerted by Rolling Stock," *Trvue Generale des Chemins de Fer*, 1967.
- [4] G. A. Hunt and Z. M. Yu, "Measurement of Lateral Resistance Characteristics for Ballasted Track BR Research Report BR-TCE-81," 1997.
- [5] Reinicke, Herrmann, and Parmentier, "Lateral Resistance Tests," DB1997.
- [6] J. van't Zand and J. Moraal, "Ballast Resistance under Three Dimensional Loading," TU Delft1996.
- [7] H. Olsson, K. J. Åström, C. Canudas de Wit, M. Gäfvert, and P. Lischinsky, "Friction models and friction compensation," *European journal of control*, vol. 4, pp. 176-195, 1998.
- [8] Corus, *Rail Products: Technical Handbook: Corus*, 2005.
- [9] Railtrack Line Specification, "Track Construction Standards," vol. RT/CE/S/006, ed, 2002.
- [10] Y. Bezin, "An Integrated Flexible Track System Model for Railway Vehicle Dynamics," PhD, Department of Engineering & Technology, Manchester Metropolitan Universtiy, Manchester, 2008.
- [11] D. M. Clark, M. McCann, and M. C. Forde, "Infrared Thromographic Investigation of Railway Track Ballast," *NDT&E international*, vol. 35, pp. 83-94, 2002.
- [12] A. Kish, G. Samavedam, and D. Wormley, "New Track Shift Safety Limits For High-speed Rail Application," in *World Congress on Railway Research*, Germany, 2001.
- [13] P. Shackleton and J. Stow, "Controlling rail vertical contact stresses," presented at the Vehicle Track Interaction, UK, 2011.
- [14] M. Burstow and M. Ryan, "VTISM: Integration of RCF modelling with T-SPA," DeltaRail, Derby2007.